

Fluorescence from rubrene single crystals: Interplay of singlet fission and energy trapping

Lin Ma,¹ Keke Zhang,² Christian Kloc,² Handong Sun,¹ Cesare Soci,¹ Maria E. Michel-Beyerle,¹ and Gagik G. Gurzadyan^{1,*}

¹*Division of Physics and Applied Physics, School of Physical and Mathematical Sciences, Nanyang Technological University, 637371 Singapore*

²*Division of Materials Science, School of Materials Science and Engineering, Nanyang Technological University, 639798 Singapore*

(Received 11 February 2013; revised manuscript received 30 April 2013; published 22 May 2013)

We have studied fluorescence in rubrene single crystals by use of fluorescence up-conversion, fluorescence anisotropy, and temperature-dependent time-resolved fluorescence techniques. Thermally activated singlet fission was demonstrated to play an important role in the quenching of two intrinsic fluorescence bands, 565 and 610 nm. At low temperatures, singlet fission is suppressed while another process, namely energy trapping, becomes pronounced. The 650 nm fluorescence originates from the hole trap states located 0.27 eV above the valence band.

DOI: [10.1103/PhysRevB.87.201203](https://doi.org/10.1103/PhysRevB.87.201203)

PACS number(s): 78.55.Kz, 72.20.Jv, 78.47.D–, 72.80.Le

Rubrene (5,6,11,12-tetraphenyltetracene) has attracted increasing attention in recent years due to its applications in organic light emitting diodes (OLEDs)¹ and organic field effect transistors (OFETs).² Rubrene single crystals are well known for their high hole mobility (up to 40 cm²/V s)^{3,4} and photoconductivity.⁵ Observations of singlet fission^{6,7} and long exciton diffusion lengths⁸ makes it potential to improve the efficiency of organic photovoltaics. Although there has been much done on the applications, some fundamental questions such as the origin of the fluorescence in rubrene single crystals remain controversial. In particular, in the case of steady-state fluorescence spectra, both experimental results and interpretations contradict depending on experimental conditions, e.g., the polarization of the excitation beam, the crystal quality, and the degree of photo-oxidation.

Rubrene crystals grown by physical vapor transport (PVT) are orthorhombic, with space group *Cmca* [Figs. 1(a)–1(d)].⁹ The reported steady-state fluorescence spectra of rubrene single crystals can be summarized into three types [Fig. 1(e)]: (1) 565 nm type. For incident light polarized parallel to the *c* axis, a strong fluorescence band centered at 565 nm dominates the fluorescence spectrum, which is explained to be due to the *M*-polarized transition¹⁰ or *c*-polarized emission.¹¹ When the excitation polarization is parallel to the *ab* facet, the 565 nm fluorescence band disappears, and instead, the fluorescence spectra are present in two other types: (2) 610 nm type. The fluorescence spectrum centered at 610 nm is usually considered as the fluorescence spectra from pristine rubrene.¹² (3) 650 nm type. Another type of fluorescence spectrum under *b* polarized excitation is centered at around 650 nm. It is disputed to be due to either the oxidation related defects,¹⁰ the band gap states,¹³ or the amorphous phase embedded in the crystal.¹²

In this work, we discuss the origin of the steady-state fluorescence in rubrene single crystals by stating the important role of singlet fission and energy trapping. The fluorescence kinetics observed was on a picosecond time scale due to the quenching by singlet fission. Thus the majority (99.9%) of the intrinsic fluorescence is quenched due to singlet fission. At low temperatures, energy trapping is observed while the thermally activated singlet fission is suppressed. The hole trap states located 0.27 eV above the valence band produce the 650 nm fluorescence band. Based on

the fluorescence anisotropy measurements, we state that the 565 nm band corresponds to the *M*-polarized transition, the 610 nm band to the *L*-polarized transition, and corroborate the 650 nm band to be due to energy trapping processes.

Rubrene single crystals were grown by the physical vapor transport (PVT) technique.¹⁴ The growing details were described in Ref. 7. All the samples used in this work were with 650 nm type steady-state fluorescence in order to study the characteristics of all fluorescence bands. A femtosecond fluorescence up-conversion spectrometer (FOG100, CDP) was used to measure the ultrafast fluorescence decay signals with 400 nm excitation femtosecond laser source (100 fs, 80 MHz). The fluorescence (540–700 nm) was collected by parabolic mirror and focused into a 0.5 mm BBO crystal (cut angle 38, ooe interaction) together with the fundamental radiation (800 nm). The resulting sum-frequency radiation (322–373 nm) after passing through a double monochromator (CDP2022D) was detected by photomultiplier-based photon-counting electronics. Temperature-dependent fluorescence spectra were recorded by the spectrofluorometer (Fluorolog-3, HORIBA Jobin Yvon), with the sample placed in a nitrogen bath cryostat (OptistatDN, Oxford Instruments). The temperature-dependent time-resolved fluorescence was measured by use of the time-correlated single-photon counting (TCSPC) technique (PicoQuant PicoHarp 300) under 450 nm excitation,⁷ combined with an exchange gas continuous flow cryostat (OptistatCF, Oxford Instruments).

In Ref. 7, we studied the singlet fission in rubrene single crystals by use of the femtosecond pump probe technique. The singlet fission rates obtained by transient absorption (TA) measurements are (2.3 ps)^{–1} and (23 ps)^{–1}. Therefore, we can expect the fluorescence lifetime of rubrene single crystal will also be on a picosecond time scale. In this work, fluorescence up-conversion measurements with 100 fs resolution were carried out in order to study the ultrafast fluorescence kinetics in rubrene. The fluorescence decays and their corresponding fit curves are shown in Fig. 2(a). All kinetics were processed biexponentially by a global fit,^{15–17} with two time constants at 2.2 and 28 ps. They correspond well with the rise time of the triplet state obtained from TA measurements.⁷ Figure 2(b) shows the amplitudes of the two time components as a function of fluorescence photon energy. For the 2.2 ps time constant, the amplitude increases while the amplitude of 28 ps decreases

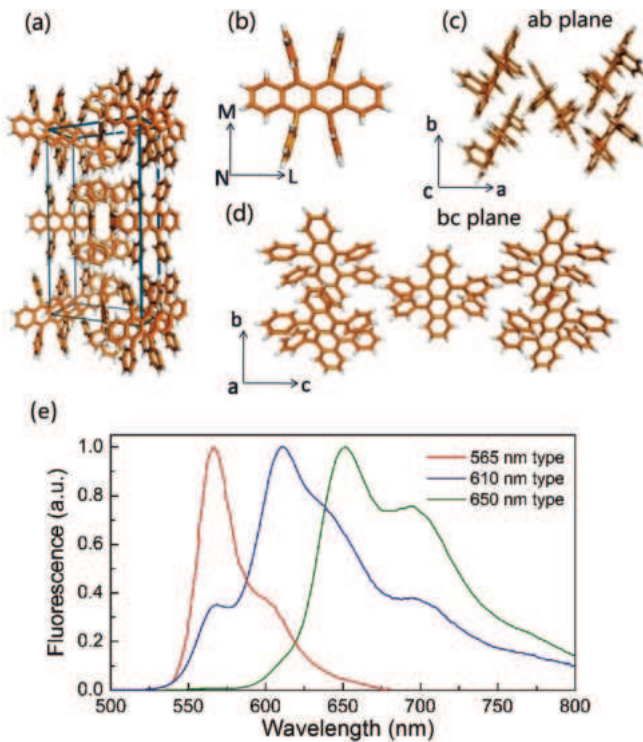


FIG. 1. (Color online) (a) Rubrene crystal structure. (b) Rubrene molecular structure. (c) Molecular packing on *ab* facet. (d) Molecular packing on *bc* facet. (e) Three types of steady-state fluorescence spectra in rubrene crystals.

with increasing emission photon energy. It implies there are two emitting states with strong spectral overlap. The faster (2.2 ps) state locates at higher energies compared with the slower (28 ps) emission state. We consider the 2.2 ps kinetics being due to direct fission from a higher vibrational state, and the 28 ps to be due to the thermally activated fission with the energy difference $\Delta = E(S_1) - 2E(T_1) = -0.05$ eV.⁷ The fluorescence lifetime of the deaerated rubrene solution is 16 ns, with quantum yield of 100%.¹⁸ Therefore, the radiative lifetime of the rubrene molecule is $\tau_{\text{rad}} = 16$ ns. In the crystals, under the assumption that singlet fission is the only quenching

process, we can estimate the singlet fission yield ϕ_{fiss} by Eq. (1):¹⁹

$$\phi_{\text{fiss}} = \frac{k_{\text{fiss}}}{k_{\text{fiss}} + k_{\text{rad}}}, \quad (1)$$

where k_{fiss} is the singlet fission rate, and k_{rad} is the radiative emission rate. For $\tau_{\text{fiss}} = 2.2$ ps, $\phi_{\text{fiss}} = 99.99\%$; and for $\tau_{\text{fiss}} = 28$ ps, $\phi_{\text{fiss}} = 99.83\%$. For the shorter emission region (540 to 600 nm), the amplitude of $\tau_{\text{fiss}} = 2.2$ ps is higher than 60%; i.e., about 99.93% of the fluorescence is quenched by singlet fission. For the longer emission region (620 to 740 nm), still 99.90% of the fluorescence is quenched. Therefore, the steady-state fluorescence spectrum reflects only 0.1% of the intrinsic fluorescence. As a consequence, if there is a low concentration (0.1%) of impurities the fluorescence spectrum will drastically be distorted. We have measured the fluorescence spectra at different positions of the same crystal, shown in the Supplemental Material, Fig. S1.²⁰ The fluorescence spectra present either the 610 or 650 nm type, which depends on the emission collecting position, indicative of the nonuniform distribution of the low-concentration “impurity.” The origin of the 650 and 700 nm fluorescence bands is discussed below.

Temperature-dependent steady-state fluorescence spectra and time-resolved fluorescence kinetics of a rubrene single crystal are shown in Fig. 3. Fluorescence intensity increases dramatically with decreasing temperature [Fig. 3(a)]. Figure 3(b) shows the fluorescence map (normalized at the maximum intensity). From the map, the peak positions of 650 and 700 nm do not change with temperature. Below 140 K, the fluorescence in the shorter emission range (560 and 610 nm bands) becomes more pronounced. There is also blueshift with decreasing temperature for the shorter emission wavelengths, which indicates that the shorter (560 and 610 nm) and longer (650 and 700 nm) fluorescence bands have different origin.

Temperature-dependent fluorescence kinetics were measured by TCSPC between 295 and 80 K. The results at 295 and 80 K are shown in Figs. 3(c) and 3(d). The results at other temperatures are presented in Fig. S2.²⁰ All fluorescence kinetics at different emission wavelengths are well fitted by two exponential components τ_1 and τ_2 . At 295 K [Fig. 3(c)], for the shorter emission range (550 to 620 nm), the main contribution (90%) is from $\tau_1 \sim 50$ ps, which is close to the time resolution of TCSPC. A small contribution (10%) is from $\tau_2 \sim 270$ ps. Based on the discussion above for the fluorescence up-conversion measurements, τ_1 corresponds to the thermally activated singlet fission. Therefore, for the 550–620 nm range the short component τ_1 becomes longer with decreasing temperature due to the suppression of singlet fission. When the temperature decreases below 140 K, a slow rise appears for the 650 and 700 nm fluorescence bands [Figs. S2(c) and S2(d)].²⁰ The rise time also becomes slower with decreasing temperature [Fig. 3(d)]. Interestingly, at temperatures below 140 K, e.g., at 80 K, the short decay of $\tau_1 = 1.3$ ns for 565 and 605 nm equals the rise time of 650 and 700 nm. This indicates an energy transfer between the shorter (donor) and longer emission ranges (acceptor). It becomes pronounced in the range of temperatures (<140 K) when singlet fission is suppressed. Arrhenius plots, i.e., dependencies of the integrated fluorescence intensity or fluorescence lifetimes versus inverse temperature are shown in Figs. 3(e)

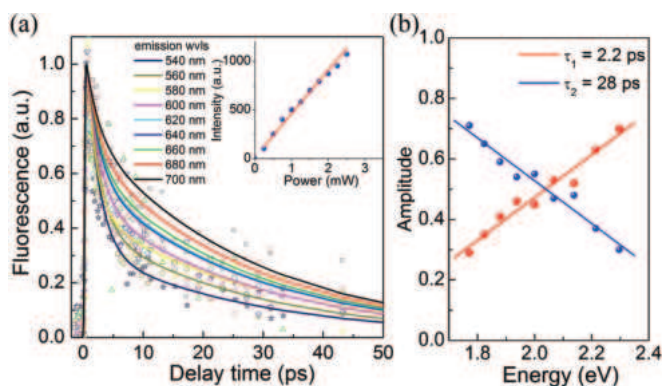


FIG. 2. (Color online) (a) Fluorescence up-conversion data (scattered) and fitting results (solid lines). Inset: Signal at 600 nm under 400 nm excitation as a function of input power, indicative of the one-photon absorption process. (b) Amplitudes of two time constants as a function of emission photon energy.

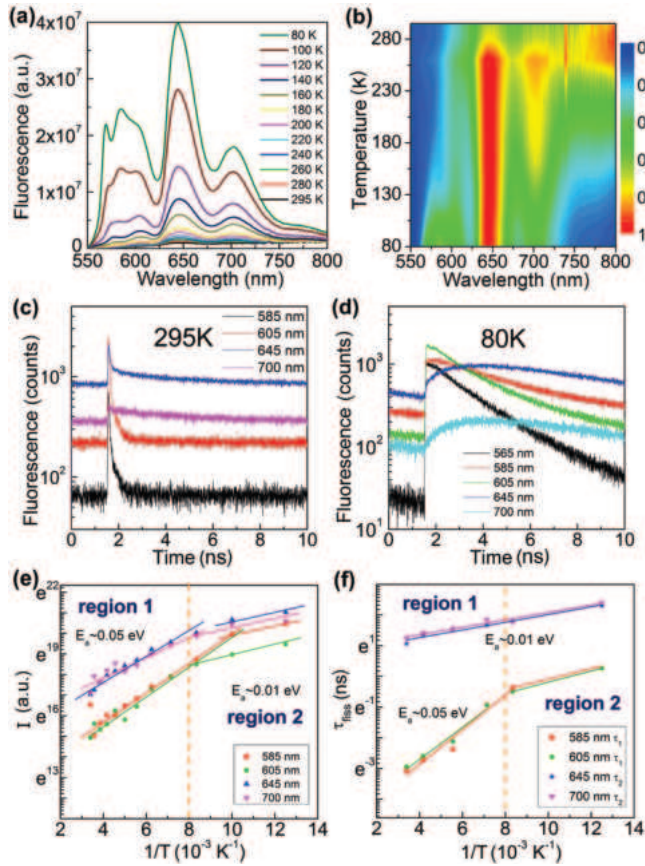


FIG. 3. (Color online) Temperature-dependent spectra of steady-state fluorescence (a) and color fluorescence map after normalization for every temperature (b). Fluorescence kinetics at 295 K (c) and 80 K (d), $\lambda_{exc} = 450$ nm. Arrhenius plot of temperature dependencies of the integrated fluorescence intensity (e) and fluorescence lifetime (f). The slopes of the linear fits (solid lines) correspond to the excitation energy E_a .

and 3(f), respectively. Five Gaussian functions with peaks at 567, 585, 608, 647, and 700 nm are used to fit the steady-state fluorescence spectra.

$\ln(I)$ and $\ln(\tau_{fiss})$ undergo a linear increase versus $1/T$. According to Arrhenius law,^{19,21}

$$k_{fiss} = A \exp\left(-\frac{E_a}{RT}\right), \quad (2)$$

where A is the pre-exponential factor, E_a is the activation energy, and R is the molar gas constant, we can obtain the activation energy E_a . From Fig. 3(e), one can clearly see two regions with different slopes of the linear dependence of $\ln(I)$ versus $1/T$. In region 1 (140 to 295 K), $E_a \sim 0.05$ eV, which corresponds to the energy difference $E(S_1) - 2E(T_1) = -0.05$ eV;⁷ i.e., the singlet fission is dominant at high temperatures. In region 2 (80 to 120 K), where the thermally activated singlet fission is suppressed, the slope becomes smaller. As mentioned above, in region 2 the energy transfer process is becoming dominant. The activation energies obtained from the temperature-dependent fluorescence kinetic data [Fig. 3(f)] show good agreement with the fluorescence intensity data [Fig. 3(e)]: $E_a \sim 0.05$ eV.

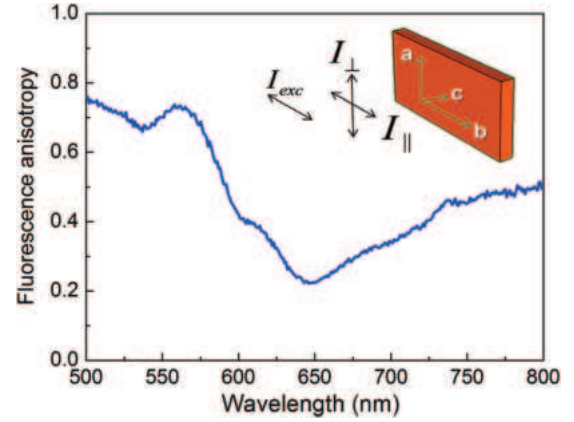


FIG. 4. (Color online) Fluorescence anisotropy of rubrene single crystal.

Now we consider the nature of the donor/acceptor system which results in 650 and 700 nm fluorescence. A possible contribution of the oxidized rubrene (rubrene peroxide²²) or the amorphous phase of rubrene embedded in the crystalline structure¹² can be ruled out: Their fluorescence maxima are at 485 and 585 nm, respectively (Fig. S3).²⁰ In rubrene crystals the hole trap states induced by oxygen defects were observed experimentally^{13,23} and discussed theoretically.²⁴ If considering that the 650 nm fluorescence originates from these trap states, then the trapping depth can be calculated as $\Delta E = 2.19$ eV (567 nm) $- 1.92$ eV (647 nm) = 0.27 eV. It agrees well with the data reported in Refs. 13 and 23 (0.25–0.27 eV). Therefore, we explain the 650 nm band as being due to the energy trapping process from the excited rubrene to the hole trap states induced by oxygen.

Tao *et al.*²⁵ studied the relaxation dynamics of photoexcited excitons in rubrene crystal by use of temperature-dependent transient absorption spectroscopy. They show that within 100 fs free excitons relax to self-trapped excitons via coherent oscillation. The decay time of the self-trapped excitons increases at low temperatures, and reaches 1 ns at 5 K. It is in agreement with our temperature-dependent fluorescence decay. However, they explain this decay as being due to exciton dissociation to charge carriers, which contradicts our fluorescence results discussed above. Mitrofanov *et al.*¹⁰ suggested that the oxygen-related defects produce an acceptor state in crystalline rubrene, which emits at 650 nm. Krellner *et al.*²³ experimentally studied the location of the oxygen-related hole trap state at 0.27 eV above the valence band. However, Podzorov *et al.*¹² claim the 650 nm fluorescence band is emitted by amorphous rubrene molecules instead of oxidized rubrene. Therefore, our results agree with the studies by Mitrofanov and Krellner that the formation of the 650 nm band is related to the oxygen-induced trap state.

It is well documented that the 565 nm band is due to M -polarized transition or c -polarized emission,^{10,11} while the 610 nm is due to L -polarized transition¹⁰ or ab -polarized emission (or depolarization of M -polarized transition).¹¹ We have measured the fluorescence anisotropy of rubrene single crystal parallel to the ab plane upon 450 nm excitation. Figure 4 shows the fluorescence anisotropy calculated by

Eq. (3):²⁶

$$r = \frac{I_{\parallel} - I_{\perp}}{I_{\parallel} + 2I_{\perp}}; \quad (3)$$

I_{\parallel} and I_{\perp} are fluorescence intensities measured in the directions parallel and perpendicular to the excitation beam, respectively. The excitation polarization was parallel to the b axis. For solid samples, under the assumption that the transition dipole moment is in the ab plane, we obtain

$$r = \frac{I \cos^2 \theta - I \sin^2 \theta}{I \cos^2 \theta + 2I \sin^2 \theta}, \quad (4)$$

where θ is the angle between the transition dipole moment and the excitation polarization direction. In Fig. 4 at 610 nm $r = 0.4$, therefore $\theta = 30^\circ$. It corresponds well to the angle between the long molecular axis L and the crystal axis c : $\alpha = 31.2^\circ$.¹⁰ Therefore, we assign the 610 nm band to the L -polarized emission. This is in full agreement with Refs. 10 and 11. At 565 nm, r reaches its maximum of 0.73. Since the crystal surface cannot be fully parallel to the polarized excitation beam, the contribution from the c -polarized transition (565 nm) will also be present under b excitation. At c -polarized fluorescence the anisotropy will be 1 since the c -polarized emission can only be collected parallel to the b axis; i.e., $I_{\perp} = 0$. The measured fluorescence intensity at 565 nm is an overlap between the M -polarized 565 nm band ($r = 1$) and the edge of the L -polarized 610 nm band ($r = 0.4$). This results in the final value of $r = 0.73$. As is well known, the energy transfer results in the depolarization of the fluorescence, and the steady-state fluorescence anisotropy of the acceptor can reach zero.^{27,28} In Fig. 4, r decreases with the increase of wavelength, and reaches the minimum at 650 nm, which confirms the energy trapping process for 650 nm emission.

Irkhin *et al.*¹¹ studied the polarization-dependent absorption and photoluminescence spectra in rubrene single crystal, and concluded that the 565 and 610 nm bands are from different vibrational levels of the first electronic excited state. The intensity difference between 565 and 610 nm bands are explained in terms of anisotropic absorption.¹¹ In our study, we emphasize the important role of singlet fission in quenching 565 and 610 nm bands; as a result, in steady-state fluorescence spectra, the 650 nm band becomes the most pronounced. We have also measured the excitation-emission matrix (EEM) fluorescence spectra for a “610 nm” type sample (Fig. S4).²⁰ We can rule out the contribution of reabsorption to the observed steady-state fluorescence spectra under ab -polarized excitation, since EEM is uniform for both 565 and 610 nm emission bands, i.e., no dependence on the excitation wavelength.

To sum up, based on the experimental results, we have interpreted the origin of fluorescence in rubrene single crystals. We demonstrated that singlet fission and energy trapping play important roles in the quenching of the excited singlet state. Fluorescence from the shorter wavelength range, 565 and 610 nm, is from the emission of pristine rubrene which undergoes ultrafast singlet fission on a time scale of 2 and 20 ps. In more detail, the 565 nm band corresponds to the M -polarized emission (along the short axis of the rubrene molecule), and 610 nm band to the L -polarized emission (along the long axis of rubrene). The longer fluorescence range, 650 and 700 nm bands, is from the hole trap states located 0.27 eV above the valence band. We emphasize that the steady-state fluorescence spectrum reflects only 0.1% of the intrinsic fluorescence. Therefore the contribution of side effects, e.g., trap states and/or different impurities, should be considered.

*gurzadyan@ntu.edu.sg

¹Y. Shao and Y. Yang, *Appl. Phys. Lett.* **86**, 073510 (2005).

²V. C. Sundar, J. Zaumseil, V. Podzorov, E. Menard, R. L. Willett, T. Someya, M. E. Gershenson, and J. A. Rogers, *Science* **303**, 1644 (2004).

³V. Podzorov, E. Menard, A. Borissov, V. Kiryukhin, J. A. Rogers, and M. E. Gershenson, *Phys. Rev. Lett.* **93**, 086602 (2004).

⁴T. Hasegawa and J. Takeya, *Sci. Technol. Adv. Mater.* **10**, 024314 (2009).

⁵H. Najafov, B. Lyu, I. Biaggio, and V. Podzorov, *Phys. Rev. B* **77**, 125202 (2008).

⁶V. V. Tarasov, G. E. Zorinians, A. I. Shushin, and M. M. Triebel, *Chem. Phys. Lett.* **267**, 58 (1997).

⁷L. Ma, K. Zhang, C. Kloc, H. Sun, M. E. Michel-Beyerle, and G. G. Gurzadyan, *Phys. Chem. Chem. Phys.* **14**, 8307 (2012).

⁸P. Irkhin and I. Biaggio, *Phys. Rev. Lett.* **107**, 017402 (2011).

⁹O. D. Jurchescu, A. Meetsma, and T. T. M. Palstra, *Acta Cryst. B* **62**, 330 (2006).

¹⁰O. Mitrofanov, C. Kloc, T. Siegrist, D. V. Lang, W.-Y. So, and A. P. Ramirez, *Appl. Phys. Lett.* **91**, 212106 (2007).

¹¹P. Irkhin, A. Rysanskiy, M. Koehler, and I. Biaggio, *Phys. Rev. B* **86**, 085143 (2012).

¹²Y. Chen, B. Lee, D. Fu, and V. Podzorov, *Adv. Mater.* **23**, 5370 (2011).

¹³O. Mitrofanov, D. V. Lang, C. Kloc, J. M. Wikberg, T. Siegrist, W.-Y. So, M. A. Sergent, and A. P. Ramirez, *Phys. Rev. Lett.* **97**, 166601 (2006).

¹⁴C. Kloc, P. G. Simpkins, T. Siegrist, and R. A. Laudise, *J. Cryst. Growth* **182**, 416 (1997).

¹⁵J. R. Knutson, J. M. Beechem, and L. Brand, *Chem. Phys. Lett.* **102**, 501 (1983).

¹⁶J. M. Beechem, M. Ameloot, and L. Brand, *Chem. Phys. Lett.* **120**, 466 (1985).

¹⁷J. M. Beechem, E. Gratton, M. Ameloot, J. R. Knutson, and L. Brand, in *Topics in Fluorescence Spectroscopy: Principles*, edited by J. R. Lakowicz, Vol. 2 (Springer, Berlin, 2003).

¹⁸H. Mattoussi, H. Murata, C. D. Merritt, Y. Iizumi, J. Kido, and Z. H. Kafafi, *J. Appl. Phys.* **86**, 2642 (1999).

¹⁹A. M. Müller, Y. S. Avlasevich, W. W. Schoeller, K. Müllen, and C. J. Bardeen, *J. Am. Chem. Soc.* **129**, 14240 (2007).

²⁰See Supplemental Material at <http://link.aps.org/supplemental/10.1103/PhysRevB.87.201203> for position-dependent fluorescence, temperature-dependent fluorescence kinetics at 120–240 K, steady-state spectra of pristine and oxidized rubrene, and the excitation-emission matrix (EEM) fluorescence spectra.

- ²¹V. K. Thorsmølle, R. D. Averitt, J. Demsar, D. L. Smith, S. Tretiak, R. L. Martin, X. Chi, B. K. Crone, A. P. Ramirez, and A. J. Taylor, *Phys. Rev. Lett.* **102**, 017401 (2009).
- ²²Ş. Erkoç, *J. Mol. Struct., Theochem* **578**, 99 (2002).
- ²³C. Krellner, S. Haas, C. Goldmann, K. P. Pernstich, D. J. Gundlach, and B. Batlogg, *Phys. Rev. B* **75**, 245115 (2007).
- ²⁴L. Tsetseris and S. T. Pantelides, *Phys. Rev. B* **78**, 115205 (2008).
- ²⁵S. Tao, N. Ohtani, R. Uchida, T. Miyamoto, Y. Matsui, H. Yada, H. Uemura, H. Matsuzaki, T. Uemura, J. Takeya, and H. Okamoto, *Phys. Rev. Lett.* **109**, 097403 (2012).
- ²⁶J. R. Lakowicz, *Principles of Fluorescence Spectroscopy*, 3rd ed. (Springer Science + Business Media, LLC, New York, 2006).
- ²⁷M. N. Berberan-Santos and B. Valeur, *J. Chem. Phys.* **95**, 8048 (1991).
- ²⁸M. Sadownik and P. Bojarski, *Chem. Phys. Lett.* **396**, 293 (2004).